2023 The 23rd International Conference on Control, Automation and Systems (ICCAS 2023)
Yeosu Venezia Hotel & Utop Marina Hotel, Yeosu, Korea, Oct. 17~20, 2023

Constrained and Unconstrained Non-Linear Control RTGC with DC Motor Based on Sliding Mode Controller

Cristian MP Napitupulu[1], Steven Bandong[2], Yul Yunazwin Nazaruddin[3], Parsaulian I. Siregar[3]

[1] Engineering Physics Program, Faculty of Industrial Technology,
Institut Teknologi Bandung, Bandung, (40132), Indonesia (13319004@mahasiswa.itb.ac.id)
[2] Engineering Physics Doctoral Program, Faculty of Industrial Technology,
Institut Teknologi Bandung, Bandung, (40132), Indonesia (bandong.steven@gmail.com)
[3] Instrumentation and Control Research Group, Department of Engineering Physics,
Institut Teknologi Bandung, Bandung, (40132), Indonesia (yul@itb.ac.id, psiregar@tf.itb.ac.id)

Abstract: The increasing exchange of goods between countries and continents necessitates efficient transportation facilities, with cargo seaports playing a vital role. Within each cargo seaport, the Rubber Tyred Gantry Crane (RTGC) is a crucial heavy equipment that requires automation to handle heavy cargo traffic and eliminate bottlenecks. Although linear control methods are commonly employed to address this issue, the system behavior is inherently nonlinear. This paper focuses on designing a non-linear control method, namely the Sliding Mode Controller (SMC), to effectively design a MIMO controller for the position, cable length, and sway of the gantry crane system. Two DC motors are used as actuators for controlling the trolley position and cable length, which hoist the container. The nonlinear gantry crane model, integrated with the nonlinear DC motor model, is elaborately derived. The designed non-linear SMC control law and sliding surface are then simulated to evaluate the control performance. Due to the limitation of the power source or DC motor specification, the paper also explores the control performance when the voltage to control RTGC is constrained to specified range. The results demonstrate that the proposed method, both on constrained and unconstrained control output, yields excellent control performance.

Keywords: Nonlinear control, Sliding mode control, Nonlinear DC motor, RTGC automation, Sway reduction

1. INTRODUCTION

The rapid advances in communication technology in this century have brought about market development, enabling sellers and buyers to make deals in just a few minutes. The increasing number of transactions demands better transportation technology to efficiently deliver goods to consumers across countries and continents. Sea transportation remains the dominant means of distributing goods in containers [1], making technology in cargo seaports a crucial aspect. The Rubber Tyred Gantry Crane (RTGC) is heavy equipment used for loading and unloading containers at container yards. Improving automation in RTGC operations is a major concern, as manual operation may lead to accidents due to lack of experience, illness, or fatigue. Furthermore, the volume of container trade worldwide has increased fourfold since 2000 [2] demonstrating its rapid growth.

Automation on RTGC focuses on two main objectives: sway control and position control. The container needs to be quickly moved to the desired position with minimal sway at the destination, ensuring ease and accuracy of placement. Some researchers have attempted to solve this problem using methods such as PID-PD [3], fuzzy-PID [4], and Robust PID based on the H-infinite method [5]. Others have aimed to optimize controller parameters through techniques like particle swarm optimization, genetic algorithms, and others [6]. However, these methods still employ linear controllers despite the RTGC system being nonlinear [7]. Therefore, it is necessary to control the RTGC using nonlinear methods.

One of the nonlinear control methods famous for its robustness against parametric uncertainties or disturbances is the Sliding Mode Controller (SMC). SMC is well-suited to solve the RTGC control problem as RTGC also encounters parametric uncertainties due to variations in container mass or wind disturbances during the container loading or unloading process. SMC has also proven to be effective in solving various control problems, such as robotic manipulator control combined with fuzzy logic [8], which performs well despite model parameter variations, and DC motor control with modified switching control to reduce chattering effects [9]. SMC has also been applied to boost converter control in PV systems under fast-varying environmental conditions [10].

In this paper, SMC will be utilized to address MIMO control problems on RTGC. The control objective encompasses not only moving the container to the desired position and minimizing sway but also controlling the cable length. The control action will be carried out by two motors that directly affect the trolley position and the cable length. Consequently, the problem falls under the category of underactuated control since the sway is not directly influenced by the actuator. The paper also provides a detailed derivation of the gantry model, considering the nonlinearities of the DC motor. Due to the limitation of the power source or DC motor specification, the paper also explores the control performance when the voltage to control RTGC is constrained to specified range. The design of the sliding surface and SMC control law, based on the nonlinear model of the DC motor and gantry crane, yields good control performance, both on constrained and unconstrained control output, which can aid researchers and practitioners in the future development of RTGC automation.

2. SYSTEM ANALYSIS

A RTGC with DC motor system can be modelled with two masses: a trolley and a container. Trolley (m_t) is attached to Motor M_1 with pulley and belt mechanism and container (m_c) is attached to Motor M_2 by a cable. Both belt and cable are assumed to be massless and non-elastic. Meanwhile, the DC motor can be modelled into two parts: electrical part (coil equivalent circuit) and mechanical part (rotator and pulley body).

Look at Fig. 1 and Fig. 2. In these two figures, the direction of the arrows indicates the direction when the variable is positive. The line N is the normal line that passes vertically through the center of mass of the trolley m_t.

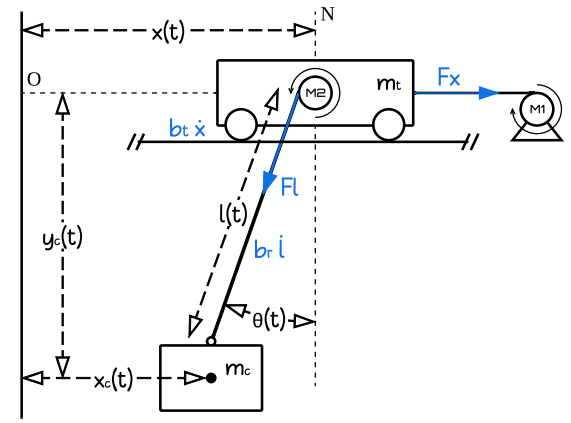

Fig. 1. RTGC with DC Motor System

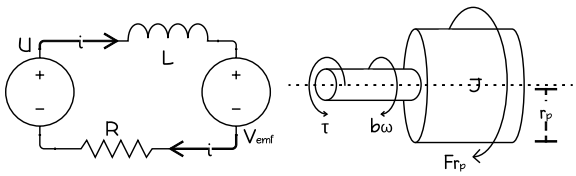

Fig. 2. DC Motor Model

The displacement of trolley denoted by $x(t)$ and the displacement of container of container denoted by $x_c(t)$ and $y_c(t)$. $l(t)$ is the length of the cable and $\theta(t)$ is the angle that is created by the cable and vertical line N while the container swaying freely along XY plane.

While operating, motor M_1 and M_2 are generating torque τ and converted into force (F) via pulley (pulley radius r_p): F_x and F_l respectively. Both F_x and F_l control the movement of trolley and container. There are also damping forces that opposing the movement of each body with damping coefficient b_t and b_r. The motor also has angular damping with coefficient b.

Each motor in the system (M_1 and M_2) will have input voltage (u_1, u_2) and intrinsic parameters such as coil inductance (L_1, L_2), coil resistance (R_1, R_2), armature inertia (J_1, J_2), angular damping coefficient (b_1, b_2), back-EMF constant (K_{e_1}, K_{e_2}), torque constant (K_{t_1}, K_{t_2}) and pulley radius (r_{p_1}, r_{p_2}) respectively.

3. SYSTEM DYNAMICS

The objective of the proposed control system design is position, cable length and sway angle which from now on $x(t)$ will be written as x, $l(t)$ as l, and $\theta(t)$ as θ.

3.1 Gantry crane

The RTGC model consist of two moving objects the trolley (m_t) and the container (m_c). Each of them has the position ($\vec{S}$), speed ($\vec{V}$), kinetic energy (K), and potential energy (P) are as follows

for Trolley (m_t)

$$\vec{S_t} = x\hat{\imath} \tag{1}$$

$$\vec{V_t} = \dot{x}\hat{\imath} \tag{2}$$

$$K_t = \frac{1}{2}m_t\left(\vec{V_t}\right)^2 = \frac{1}{2}m_t\dot{x}^2 \tag{3}$$

$$P_t = m_t g \cdot \vec{S_t} \cdot \hat{\jmath} = 0 \tag{4}$$

for Container (m_c)

$$\vec{S_c} = \left(x - l\sin(\theta)\right)\hat{\imath} - l\cos(\theta)\hat{\jmath} \tag{5}$$

$$\vec{V_c} = \begin{pmatrix}\left(\dot{x} - \dot{l}\sin(\theta) - l\dot{\theta}\cos(\theta)\right)\hat{\imath} \\ +\left(l\dot{\theta}\sin(\theta) - \dot{l}\cos(\theta)\right)\hat{\jmath}\end{pmatrix} \tag{6}$$

$$K_c = \frac{1}{2}m_c\left(\vec{V_t}\right)^2$$

$$K_c = \begin{pmatrix}\frac{1}{2}m_c\dot{x}^2 + \frac{1}{2}m_c\dot{l}^2 + \frac{1}{2}m_c l^2\dot{\theta}^2 \\ -m_c\dot{x}\dot{l}\sin(\theta) - m_c\dot{x}l\dot{\theta}^2\cos(\theta)\end{pmatrix} \tag{7}$$

$$P_c = m_c g \cdot \vec{S_c} \cdot \hat{\jmath} = -m_c g l\cos(\theta) \tag{8}$$

From the combined kinetic and potential energy, the Lagrangian (L) is obtained as follows

$$L = K_t + K_c - P_t - P_c \tag{9}$$

Additionally, the Lagrange Equation can be obtained for each coordinate x, l, and θ as presented below.

$$\frac{d}{dt}\left(\frac{dL}{d\dot{x}}\right) - \frac{dL}{dx} = F_x - b_t\dot{x} \tag{10}$$

$$\frac{d}{dt}\left(\frac{dL}{d\dot{l}}\right) - \frac{dL}{dl} = F_l - b_r\dot{l} \tag{11}$$

$$\frac{d}{dt}\left(\frac{dL}{d\dot{\theta}}\right) - \frac{dL}{d\theta} = 0 \tag{12}$$

Substituting eqs. (3), (4), (7), (8) into eq. (9) and solve for F_x, F_l, and 0 for eqs. (10), (11), and (12), the results are then presented in the following equations

$$F_x = \begin{pmatrix}(m_t + m_c)\ddot{x} - m_c\sin(\theta)\ddot{l} \\ -m_c l\cos(\theta)\ddot{\theta} + b_t\dot{x} \\ -2m_c\cos(\theta)\dot{\theta}\dot{l} + m_c l\sin(\theta)\dot{\theta}^2\end{pmatrix} \tag{13}$$

$$F_l = \begin{pmatrix}-m_c\sin(\theta)\ddot{x} + m_c\ddot{l} + b_r\dot{l} \\ -m_c l\dot{\theta}^2 - m_c g\cos(\theta)\end{pmatrix} \tag{14}$$

$$0 = -\cos(\theta)\ddot{x} + l\ddot{\theta} + 2\dot{l}\dot{\theta} + g\sin(\theta) \tag{15}$$

Rewrite eq. (15) to get $\ddot{\theta}$ as follows

$$\ddot{\theta} = \frac{\cos(\theta)\ddot{x} - 2\dot{l}\dot{\theta} - g\sin(\theta)}{l} \tag{16}$$

substituting eq. (16) into eq. (13) yields

$$F_x = \begin{pmatrix}(m_t + m_c\sin^2(\theta))\ddot{x} + b_t\dot{x} \\ -m_c\sin(\theta)\ddot{l} + m_c l\sin(\theta)\dot{\theta}^2 \\ +m_c g\sin(\theta)\cos(\theta)\end{pmatrix} \tag{17}$$

3.2 DC motor

From now on, symbol L is not representing Lagrangian but the coil inductance of DC motor instead.

From Fig. 2, these two equations are obtained

$$u - L\frac{di}{dt} - Ri - V_{emf} = 0 \tag{18}$$

$$\tau - b\omega - Fr_p = J\dot{\omega} \tag{19}$$

The rotating rotor of a DC motor induces back-EMF in the coil proportional to its angular speed. The coil's electric current generates a magnetic field that interacts with the stator's permanent magnet, resulting in torque on the rotor. These relations can be formulated as follows

$$V_{emf} = K_e\,\omega \tag{20}$$

$$\tau = K_t i \tag{21}$$

where u is the input voltage, L is coil inductance, R is coil resistance, i is the electric current inside the coil, V_{emf} is the back-EMF, τ is torque on rotator, b is damping coefficient of the DC motor, ω is angular speed of rotator, F is load force, r_p is pulley radius, J is inertia of rotator and pulley, K_e is EMF constant, and K_t is torque constant.

Eqs. (22) and (23) are obtained by substituting eq. (20) into eq. (18) and eq. (21) into eq. (19) and then, performs a Laplace transform to the resulting two equations.

$$U(s) - K_e\Omega(s) = (Ls + R)I(s) \tag{22}$$

$$I(s) = \frac{(Js + b)\Omega(s) + r_pF(s)}{K_t} \tag{23}$$

Substituting eq. (23) into eq. (22) and rearranging to get eq. (24).

$$U(s) = \left(\frac{(Ls + R)(Js + b)}{K_t} + K_e\right)\Omega(s) + \frac{(Ls + R)r_p}{K_t}F(s) \tag{24}$$

On pulley, applies equation $v = \omega r_p$, where v is tangential velocity of the pulley. Perform Laplace transform to that equation and solve for $\Omega(s)$.

$$\Omega(s) = \frac{V(s)}{r_p} \tag{25}$$

Substitute eq. (25) into eq. (24) and performs inverse Laplace transform to the resulting equation, such that the following expression is obtained

$$u = \frac{LJ}{K_tr_p}\ddot{v} + \frac{Lb + RJ}{K_tr_p}\dot{v} + \left(\frac{Rb}{K_tr_p} + \frac{K_e}{r_p}\right)v + \frac{Lr_p}{K_t}\dot{F} + \frac{Rr_p}{K_t}F \tag{26}$$

3.3 Gantry crane and DC motor integration

Eq. (26) is used for motor M_1 and M_2. Therefore, it is necessary to make variable adjustments are needed for each motor. Since motor M_1 is responsible for generating F_x, set $F = F_x$, $v = \dot{x}$, $u = u_1$, $L = L_1$, $R = R_1$, $J = J_1$, $b = b_1$, $r_p = r_{p_1}$, $K_e = K_{e_1}$, and $K_t = K_{t_1}$ to eq. (26) for motor M_1.

Additionally, since motor M_2 is responsible for generating F_l, set $F = F_l$, $v = \dot{l}$, $u = u_2$, $L = L_2$, $R = R_2$, $J = J_2$, $b = b_2$, $r_p = r_{p_2}$, $K_e = K_{e_2}$, and $K_t = K_{t_2}$ to eq. (26) for motor M_2.

Then, substitute eq. (14) and (17) into eq. (26) such that two equations obtained. Eq. (27) for motor M_1 and eq. (28) for motor M_2.

$$u_1 = a_{11}\ddot{x} + a_{12}\ddot{l} + b_{11}\dot{x} + b_{12}\dot{l} + c_{11}x + d_1\ddot{\theta} + e_1\dot{\theta} + f_1 \tag{27}$$

$$u_2 = a_{21}\ddot{x} + a_{22}\ddot{l} + b_{21}\dot{x} + b_{22}\dot{l} + c_{22}\dot{l} + d_2\ddot{\theta} + e_2\dot{\theta} + f_2 \tag{28}$$

Rewrite eq. (27) and (28) into matrix form as presented below.

$$\begin{bmatrix}u_1\\u_2\end{bmatrix} = \begin{bmatrix}a_{11} & a_{12}\\a_{21} & a_{22}\end{bmatrix}\begin{bmatrix}\ddot{x}\\\ddot{l}\end{bmatrix} + \begin{bmatrix}b_{11} & b_{12}\\b_{21} & b_{22}\end{bmatrix}\begin{bmatrix}\dot{x}\\\dot{l}\end{bmatrix} + \begin{bmatrix}c_{11} & 0\\0 & c_{22}\end{bmatrix}\begin{bmatrix}x\\l\end{bmatrix} + \begin{bmatrix}d_1\\d_2\end{bmatrix}\ddot{\theta} + \begin{bmatrix}e_1\\e_2\end{bmatrix}\dot{\theta} + \begin{bmatrix}f_1\\f_2\end{bmatrix} \tag{29}$$

$$u = A\ddot{q} + B\ddot{q} + C\dot{q} + D\ddot{\theta} + E\dot{\theta} + F \tag{30}$$

Rewrite eq. (30) to obtain eq. (31)

$$\ddot{q} = A^{-1}\left(u - B\ddot{q} - C\dot{q} - D\ddot{\theta} - E\dot{\theta} - F\right) \tag{31}$$

where

$$u = \begin{bmatrix}u_1\\u_2\end{bmatrix};\ q = \begin{bmatrix}x\\l\end{bmatrix};\ A = \begin{bmatrix}a_{11} & a_{12}\\a_{21} & a_{22}\end{bmatrix};\ B = \begin{bmatrix}b_{11} & b_{12}\\b_{21} & b_{22}\end{bmatrix};$$

$$C = \begin{bmatrix}c_{11} & 0\\0 & c_{22}\end{bmatrix};\ D = \begin{bmatrix}d_1\\d_2\end{bmatrix};\ E = \begin{bmatrix}e_1\\e_2\end{bmatrix};\ F = \begin{bmatrix}f_1\\f_2\end{bmatrix};$$

$$a_{11} = \frac{L_1J_1}{K_{t_1}r_{p_1}} + \frac{L_1r_{p_1}}{K_{t_1}}(m_t + m_c\,sin^2(\theta));$$

$$a_{12} = -\frac{L_1r_{p_1}}{K_{t_1}}m_c\,sin(\theta);\ a_{21} = -\frac{L_2r_{p_2}}{K_{t_2}}m_c\,sin(\theta);$$

$$a_{22} = \frac{L_2J_2}{K_{t_2}r_{p_2}} + \frac{L_2r_{p_2}}{K_{t_2}}m_c;$$

$$b_{11} = \frac{L_1b_1 + R_1J_1}{K_{t_1}r_{p_1}} + \frac{L_1r_{p_1}}{K_{t_1}}m_c\,sin(2\theta)\,\dot{\theta} + \frac{L_1r_{p_1}}{K_{t_1}}b_t + \frac{R_1r_{p_1}}{K_{t_1}}(m_t + m_c\,sin^2(\theta));$$

$$b_{12} = -\left(\frac{L_1r_{p_1}}{K_{t_1}}m_c\,cos(\theta)\,\dot{\theta} + \frac{R_1r_{p_1}}{K_{t_1}}m_c\,sin(\theta)\right);$$

$$b_{21} = -\left(\frac{L_2r_{p_2}}{K_{t_2}}m_c\,cos(\theta)\,\dot{\theta} + \frac{R_2r_{p_2}}{K_{t_2}}m_c\,sin(\theta)\right);$$

$$b_{22} = \frac{L_2b_2 + R_2J_2}{K_{t_2}r_{p_2}} + \frac{L_2r_{p_2}}{K_{t_2}}b_r + \frac{R_2r_{p_2}}{K_{t_2}}m_c;$$

$$c_{11} = \frac{R_1b_1}{K_{t_1}r_{p_1}} + \frac{K_{e_1}}{r_{p_1}} + \frac{R_1r_{p_1}}{K_{t_1}}b_t;$$

$$c_{22} = \frac{R_2b_2}{K_{t_2}r_{p_2}} + \frac{K_{e_2}}{r_{p_2}} + \frac{R_2r_{p_2}}{K_{t_2}}b_r;$$

$$d_1 = 2\frac{L_1r_{p_1}}{K_{t_1}}m_cl\,sin(\theta)\,\dot{\theta};\ d_2 = -2\frac{L_2r_{p_2}}{K_{t_2}}m_cl\dot{\theta};$$

$$e_1 = \frac{L_1r_{p_1}}{K_{t_1}}m_cl\,cos(\theta)\,\dot{\theta}^2 + \frac{r_{p_1}}{K_{t_1}}m_c\,sin(\theta)\,(L_1\dot{l} + R_1l)\dot{\theta} + \frac{L_1r_{p_1}}{K_{t_1}}m_cg\,cos(2\theta);$$

$$e_2 = -\frac{r_{p_2}}{K_{t_2}}m_c(L_2\dot{l} + R_2l)\dot{\theta} + \frac{L_2r_{p_2}}{K_{t_2}}m_cg\,sin(\theta);$$

$$f_1 = \frac{R_1 r_{p_1}}{K_{t_1}} m_c g \frac{sin(2\theta)}{2}; f_2 = -\frac{R_2 r_{p_2}}{K_{t_2}} m_c g\, cos(\theta).$$

4. SLIDING MODE CONTROLLER

The main objectives of the RTGC with DC motor system are threefold: (1) achieving a specific position (x_d) for the container, (2) hoisting or lowering the container (l_d), and (3) minimize excessive swaying of the container.

To achieve this goal, the desired value $q_d = [x_d, l_d]^T$ and $\theta_d = 0$ will be set. From this desired value, error functions can be derived for each parameter as presented below.

$$e_1 = q - q_d; e_2 = \theta - \theta_d = \theta$$

To enable sliding mode control, it is necessary to define a sliding surface. For this system, the sliding surface s is chosen as follows

$$s = \alpha e_1 + \beta \dot{e}_1 + \ddot{e}_1 + \lambda e_2$$
$$s = \alpha(q - q_d) + \beta \dot{q} + \ddot{q} + \lambda\, \theta \quad (32)$$

where

$$s = \begin{bmatrix} s_1 \\ s_2 \end{bmatrix}; \alpha = \begin{bmatrix} \alpha_1 & 0 \\ 0 & \alpha_2 \end{bmatrix}; \beta = \begin{bmatrix} \beta_1 & 0 \\ 0 & \beta_2 \end{bmatrix}; \lambda = \begin{bmatrix} \lambda_1 \\ \lambda_2 \end{bmatrix}.$$

Deriving eq. (32) yields eq. (33)

$$\dot{s} = \alpha \dot{q} + \beta \ddot{q} + \dddot{q} + \lambda \dot{\theta} \quad (33)$$

Substitute eq. (31) into eq. (33)

$$\dot{s} = \alpha \dot{q} + \beta \ddot{q} + A^{-1}\left(u - B\ddot{q} - C\dot{q} - D\ddot{\theta} - E\dot{\theta} - F\right) + \lambda \dot{\theta}$$

Set $\dot{s} = 0$ and rearrange to get expression below

$$u = (B - A\beta)\ddot{q} + (C - A\alpha)\dot{q} + D\ddot{\theta} + (E - A\lambda)\dot{\theta} + F$$

In a sliding mode controller, a reaching mode (u_{RM}) is required as an initialization step to guide the system towards the selected sliding surface. For this system, the reaching mode is chosen as presented below

$$u_{RM} = -k \cdot sign(s)$$

where $k = [k_1, k_2]^T$ and $sign(s)$ is a function that return the sign of every element of s.

Finally, the complete control law for non-linear RTGC with DC motor system can be expressed in eq. (34).

$$u_{SMC} = u + u_{RM}$$
$$u_{SMC} = \begin{pmatrix} (B - A\beta)\ddot{q} + (C - A\alpha)\dot{q} \\ +D\ddot{\theta} + (E - A\lambda)\dot{\theta} \\ +F - k \cdot sign(s) \end{pmatrix} \quad (34)$$

5. RESULTS AND DISCUSSION

To evaluate the performance of the model and sliding mode controller, 2 scenarios will be conducted, namely the unconstrained control law scenario and the constrained control law scenario. Both scenarios aim to move the container from an initial position $x_0 = 0$ and $l_0 = 1.5m$ to desired position $x_d = 1m$ and cable length $l_d = 0.5m$. The selection of initial and desired position allows for observing the action of the control law as it moves the trolley (m_t) and hoists the container (m_c) simultaneously, while minimizing the sway angle (θ).

In the constrained control law scenario, the control law will be constrained by a limit value of $u_{limit} = 4.2V$. This value represents a typical limit for a single celled Li-Po battery at full charge, simulating real life constraints. Other than this constraint, both scenarios will utilize the same set of parameters as follows

$$m_c = 2.0kg;\ m_t = 2.0kg; b_t = 10Nsm^{-1};$$
$$b_r = 10Nsm^{-1};\ g = 9.81ms^{-2};\ L_1 = 1.5mH;$$
$$R_1 = 10\Omega;\ J_1 = 0.0005Nm^2;\ b_1 = 0.0004Nms;$$
$$r_{p_1} = 0.01m;\ K_{e_1} = 0.05Vs;\ K_{t_1} = 0.05NmA^{-1};$$
$$L_2 = 2.5mH; R_2 = 1.2\Omega; J_2 = 0.0007Nm^2;$$
$$b_2 = 0.0004Nms;\ r_{p_2} = 0.01m;\ K_{e_2} = 0.08Vs;$$
$$K_{t_2} = 0.08NmA^{-1}; \alpha_1 = 0.5; \alpha_2 = 2.5; \beta_1 = 2.0;$$
$$\beta_2 = 5.0; \lambda_1 = 15.0; \lambda_2 = 1.0; k_1 = 0.003; k_2 = 0.01.$$

For the first scenario (Fig. 3 to Fig. 7), the sliding mode controller managed to make the system achieve the desired value (x_d, l_d) while minimizing the sway angle and achieving a fast settling time. In Fig. 6, the control law u_1 is observed to oscillate to reduce the sway angle. Furthermore, a few seconds before settling, θ exhibits a negative value, indicating that the container is oscillating to the right of the normal line N depicted in Fig. 1. This behavior is attributed to the deceleration of the trolley, as shown in Fig. 3.

For the second scenario (Fig. 8 to Fig. 12), unconstrained control law, control law u_1 also seems to be trying to reduce the sway angle by oscillating its value but u_1 and u_2 are clipped at $u_{limit} = 4.2V$ as shown in Fig. 11 and Fig. 12. In Fig. 9, the rate of change in the length of the cable is stuck at a value of $0.12ms^{-1}$ so that the duration of hoisting the container becomes longer. This makes the performance of the sliding mode controller not as good as the unconstrained scenario. Even so, the system can still go to the desired value properly.

In both scenarios, u_2 does not settle at 0 like u_1 did, but instead, it settles at approximately -3V. This observation aligns with research's objectives expectation, as it is apparent that the motor M_2 need to remain active to maintain the container's position and prevent it from falling.

Even though both scenarios show good results, of course the unconstrained scenario's result are better. As a form of quantification of the performance of the two scenarios, a performance table has been presented in Table 1. This table shows the rise time for x and l, settling time for x, l, and θ, as well as the RMSE of the three at steady state.

Rise time is calculated as the time difference when x and l reach a value of 10% and 90% error at time $t = 0$. Settling time is calculated as the time required to have a stable value below 2% of the setpoint (q_d). For θ, because the value of θ_d is 0, a maximum error limit of 0.057 degrees (0.001 rads) is created. Additionally, RMSE at steady state is calculated since of x, l, and θ enter the steady state phase $(t \geq t_{settling})$.

Based on Table 1, it can be inferred that the performance of Sliding Mode Controller in the unconstrained scenario outperformed the constrained scenario. Although the RMSE values are similar, the unconstrained scenario demonstrates faster rise time and settling time compared to the constrained scenario.

Table 1. Sliding Mode Controller Performance for Each Scenario

Scenario	Displacement *(x)*			Cable length *(l)*			Sway angle *(θ)*	
	Rise time *(s)*	Settling time *(s)*	RMSE *(m)*	Rise time *(s)*	Settling time *(s)*	RMSE *(m)*	Settling time *(s)*	RMSE *(degree)*
Unconstrained	6.31	10.436	0.005	3.98	7.519	0.005	9.786	0.018
Constrained	7.971	12.453	0.006	6.878	10.751	0.006	11.5	0.019

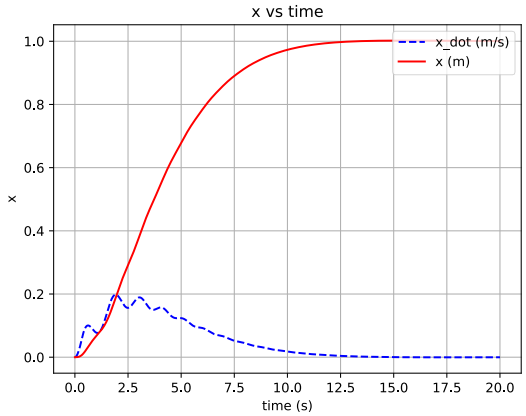

Fig. 3. Unconstrained *x vs time*

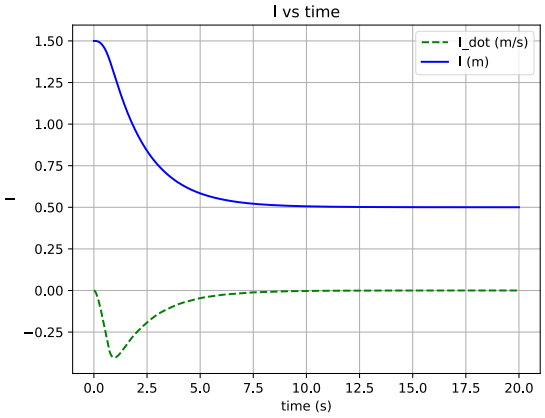

Fig. 4. Unconstrained *l vs time*

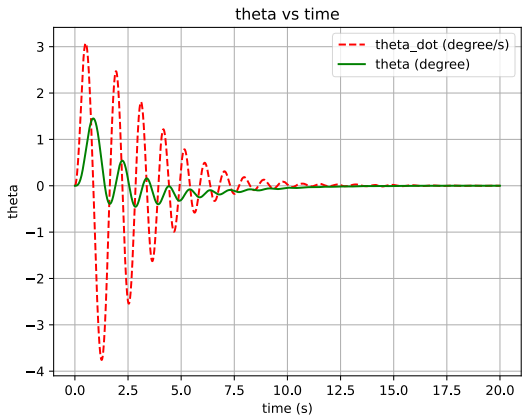

Fig. 5. Unconstrained θ *vs time*

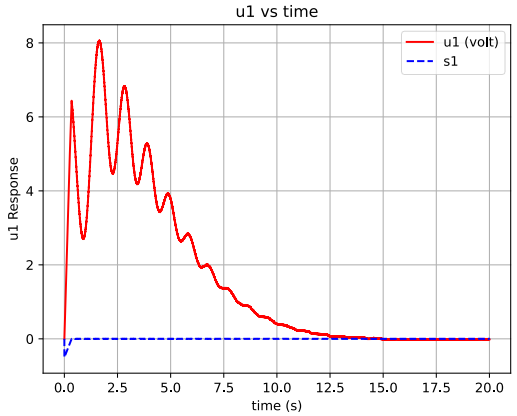

Fig. 6. Unconstrained u_1 *vs time*

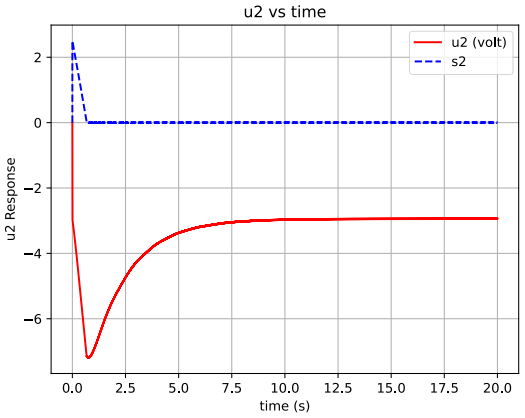

Fig. 7. Unconstrained u_2 *vs time*

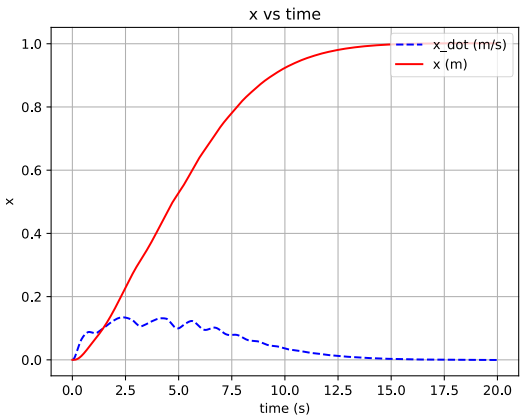

Fig. 8. Constrained *x vs time*

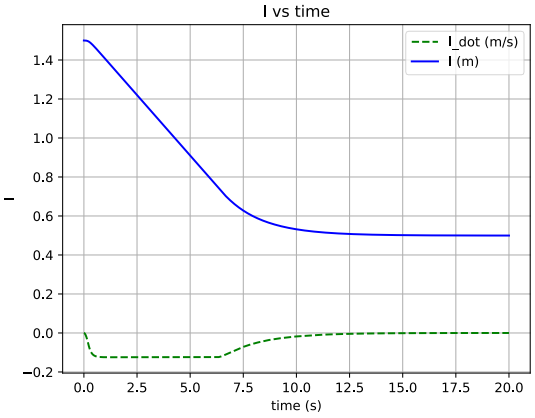

Fig. 9. Constrained l *vs time*

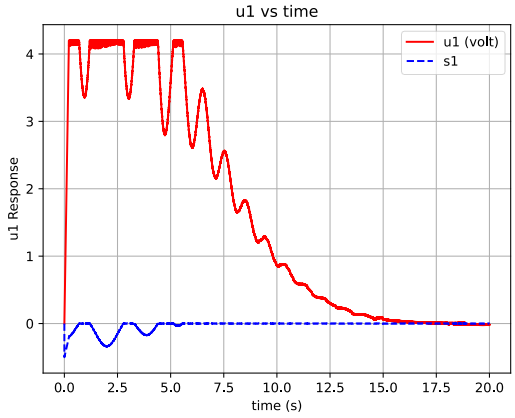

Fig. 11. Constrained u_1 *vs time*

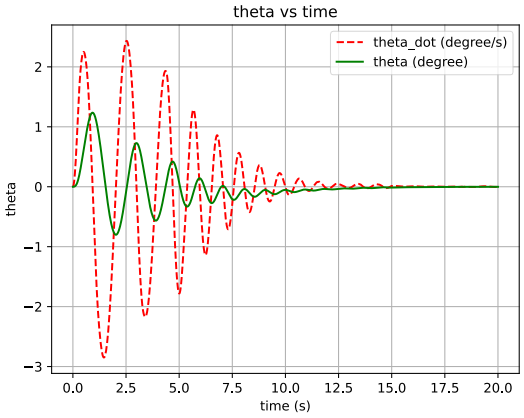

Fig. 10. Constrained θ *vs time*

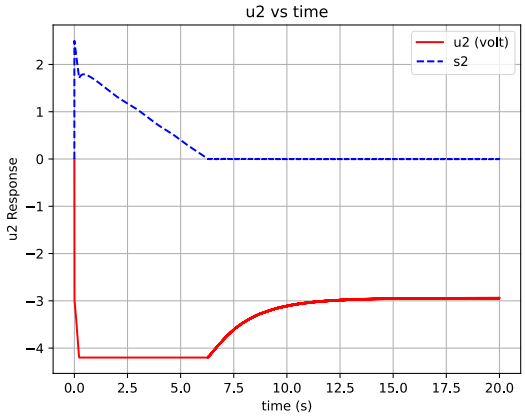

Fig. 12. Constrained u_2 *vs time*

CONCLUSION

The paper addresses the MIMO problem in controlling RTGC to minimize the sway angle during the movement towards the desired container position and cable length adjustment. Two motors are utilized for controlling the trolley's position and hoisting the cable to the container. The nonlinear control method using SMC and its sliding surface have been designed to account for the nonlinearities presented by the DC motor and RTGC model. The paper also considers the unconstrained and constrained control outputs, taking into account power source limitations and DC motor specifications. The results indicate that both constrained and unconstrained approaches yield good results in terms of rise time, settling time, and RMSE. While the unconstrained approach slightly outperforms the constrained approach, the latter is more applicable as it respects the limitations imposed by the actuator or power source. Future research will focus on enhancing the control performance of the SMC on RTGC and applying the developed method to a laboratory-scale RTGC prototype.

ACKNOWLEDGEMENTS

The Research supported by Institut Teknologi Bandung International Research Collaboration Program 2022, and Doctoral Dissertation Research 2023 from the Ministry of Education, Culture, Research, and Technology, Indonesia. S. Bandong is supported by the Indonesia Endowment Fund for Education (LPDP), Indonesia.

REFERENCES

[1] R. J. Sanchez, J. Hoffmann, A. Micco, G. V Pizzolitto, M. Sgut, and G. Wilmsmeier, "Port efficiency and international trade: port efficiency as a determinant of maritime transport costs," Maritime economics & logistics, vol. 5, pp. 199–218, 2003.

[2] 2023 The World Bank Group, "Container port traffic (TEU: 20-foot equivalent units)," https://data.worldbank.org/indicator/IS.SHP.GOOD.TU, Jun. 29, 2023.

[3] S. Y. Syed Hussien, H. I. Jaafar, R. Ghazali, and N. R. Abdul Razif, "The effects of auto-tuned method in PID and PD control scheme for gantry crane system," International Journal of Soft Computing and Engineering (IJSCE), vol. 4, no. 6, 2015.

[4] F. Zheng, C. H. Yang, G. Hao, K. C. Wang, and H. L. Hong, "Vision-based fuzzy proportional–integral–derivative tracking control scheme for

gantry crane system," Sensors and Materials, vol. 33, no. 9, 2021, doi: 10.18494/SAM.2021.3403.

[5] S. Bandong, Y. Y. Nazaruddin, and E. Joelianto, "Optimal RTGC Controller using Robust PID H∞ Integral-Backstepping under Payload Mass and Rope Length Uncertainties," in 2022 17th International Conference on Control, Automation, Robotics and Vision (ICARCV), 2022, pp. 18–23.

[6] S. Bandong, R. C. Kirana, Y. Y. Nazaruddin, and E. Joelianto, "Optimal Gantry Crane PID Controller Based on LQR with Prescribed Degree of Stability by Means of GA, PSO, and SA," in 7th International Conference on Electric Vehicular Technology, ICEVT 2022 - Proceeding, 2022. doi: 10.1109/ICEVT55516.2022.9925018.

[7] H. I. Jaafar, Z. Mohamed, J. J. Jamian, A. F. Z. Abidin, A. M. Kassim, and Z. A. Ghani, "Dynamic Behaviour of a Nonlinear Gantry Crane System," Procedia Technology, vol. 11, 2013, doi: 10.1016/j.protcy.2013.12.211.

[8] A. Ashagrie, A. O. Salau, and T. Weldcherkos, "Modeling and control of a 3-DOF articulated robotic manipulator using self-tuning fuzzy sliding mode controller," Cogent Eng, vol. 8, no. 1, 2021, doi: 10.1080/23311916.2021.1950105.

[9] A. Ma'arif and A. Çakan, "Simulation and arduino hardware implementation of dc motor control using sliding mode controller," Journal of Robotics and Control (JRC), vol. 2, no. 6, 2021, doi: 10.18196/jrc.26140.

[10] R. S. Inomoto, J. R. B. D. A. Monteiro, and A. J. S. Filho, "Boost Converter Control of PV System Using Sliding Mode Control With Integrative Sliding Surface," IEEE J Emerg Sel Top Power Electron, vol. 10, no. 5, 2022, doi: 10.1109/JESTPE.2022.3158247.J.